Determination of some basic physical parameters of SnO based on SnO/Si pn heterojunctions

Xiuxia Li, Lingyan Liang, Hongtao Cao, Ruifeng Qin, Hongliang Zhang, Junhua Gao, and Fei Zhuge

Citation: Applied Physics Letters **106**, 132102 (2015); doi: 10.1063/1.4916664
View online: http://dx.doi.org/10.1063/1.4916664
View Table of Contents: http://scitation.aip.org/content/aip/journal/apl/106/13?ver=pdfcov
Published by the AIP Publishing

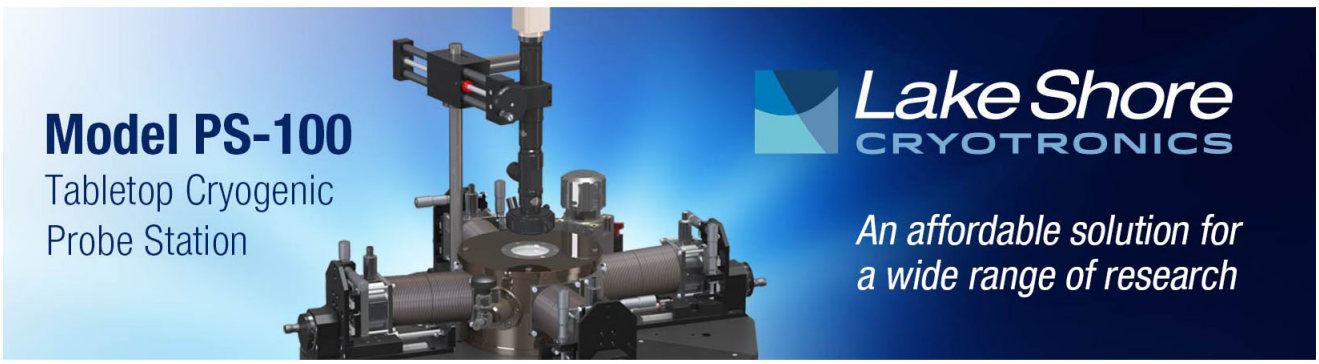

Determination of some basic physical parameters of SnO based on SnO/Si pn heterojunctions

Xiuxia Li,[1,2] Lingyan Liang,[2,a)] Hongtao Cao,[2,a)] Ruifeng Qin,[2] Hongliang Zhang,[2] Junhua Gao,[2] and Fei Zhuge[2]
[1]*Department of Physics, North University of China, Taiyuan 030051, People's Republic of China*
[2]*Division of Functional Materials and Nano Devices, Ningbo Institute of Material Technology and Engineering, Chinese Academy of Sciences, Ningbo 315201, People's Republic of China*

(Received 12 February 2015; accepted 20 March 2015; published online 30 March 2015)

P-SnO/n-Si heterojunctions were constructed by using e-beam evaporation in combination with ultra-violet lithography technique. The current-voltage and capacitance-voltage characteristics of the pn heterojunctions were systematically investigated, through which the diode parameters, such as the turn-on voltage, forward-to-reverse current ratio, series resistance, ideality factor, and build-in voltage, were also determined. In particular, the pn heterojunctions presented a relatively good electrical rectifying behavior, with a forward-to-reverse current ratio up to 58 ± 5 at ± 2.0 V. The relative permittivity and work function of the SnO films were measured to be 18.8 ± 1.7 and 4.3 eV, respectively. The energy band diagram of the heterojunctions was depicted in detail, which can interpret the rectifying behavior very well. © *2015 AIP Publishing LLC*.
[http://dx.doi.org/10.1063/1.4916664]

Oxide semiconductors are one of backbone materials for practical applications such as gas or gamma radiation sensor, solar cell, lithium rechargeable battery, photocatalyst, electronic switch for flat-panel displays, and so on.[1–6] However, most of oxide semiconductors show n-type conduction. Even though the presence of a limited number of p-type oxides, their p-type conductivity still lags behind with respect to the n-type counterparts. So the obvious unbalanced development between the n-type and p-type oxide semiconductors severely limits the potential applications in oxide-based complementary devices/circuits, optoelectronic devices, etc. Tin monoxide (SnO), as an intrinsic p-type oxide semiconductor, has gained attractive attentions in the past few years. SnO has been studied as the anode material of lithium rechargeable batteries,[7] the channel material of p-type or ambipolar thin-film transistors,[8–12] and the p-type semiconductor material in the pn junctions.[13–16]

The pn junctions usually serve as "building blocks" in the semiconductor devices such as solar cells, light-emitting diodes, photodetectors, rectifier diodes, and bipolar transistors. According to the literature, p-SnO/n-SnO,[13] p-SnO/n-ZnO,[14,15] and p-SnO/n-SnO_2[16] junctions have been studied previously. The energy band diagrams[14,16] of the pn junctions were depicted by using the optical direct bandgap (2.5–3.4) of SnO,[16,17] regardless of the fact that SnO has an indirect fundamental gap (0.5–0.7 eV).[8,18] Basically, the fundamental gap should be applied in the energy band diagram of the pn junctions, because that the energy band diagram of a pn junction describes the electrical behaviors, e.g., the band offsets for electron and hole transport. In this work, p-SnO/n-Si heterojunctions were constructed, and their energy band diagram was depicted based on the basic physical parameters derived from current-voltage (I-V) and capacitance-voltage (C-V) measurements.

SnO thin films were deposited on n^+ Si ⟨100⟩ silicon wafers at room temperature using an e-beam evaporation system with high-purity SnO_2 powders as the source material. The growth mechanism was presented elsewhere.[19] The nominally undoped SnO films, ~130 nm in thickness, were prepared with a deposition rate of 1.8 nm/min. Before being loaded into the deposition chamber, the silicon substrates were cleaned by organic solvents (acetone and alcohol) and deionized H_2O. Subsequently, the wafers were dipped into a 5% HF solution for 5 min to remove the surface oxide film. Each layer in the heterojunction was defined by standard lithography, as schematically shown in the inset of Figure 1. The Ni/Au films were evaporated both on silicon wafer and SnO film as electrodes. The lift-off process was carried out by an ultrasonic-assisted cleaning in the organic solvents. After that, the samples were immediately treated by rapid

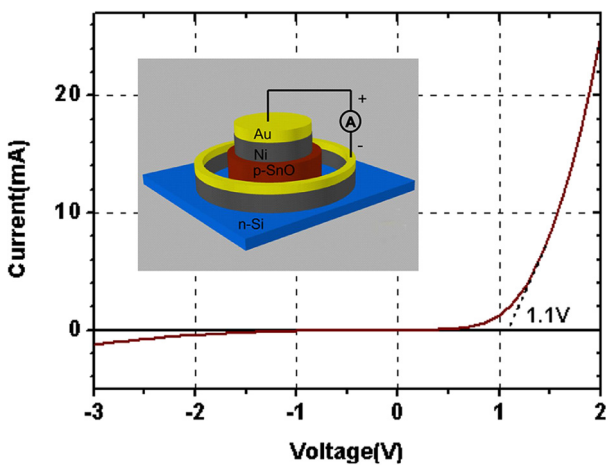

FIG. 1. I-V characteristics of the p-SnO/n-Si heterojunction and the corresponding device structure diagram (inset).

a)Authors to whom correspondence should be addressed. Electronic addresses: lly@nimte.ac.cn and h_cao@nimte.ac.cn

thermal annealing at 350 °C for 10 min in argon ambient. The influence of the annealing temperature on the electrical properties of the junctions is given in the supplementary material (Figure S1).[33]

The thickness of SnO films were determined by a spectroscopic ellipsometer (M-2000DI, J.A. Woollam Co., Inc.). The work function of the SnO films was measured by the ultraviolet photoelectron spectroscopy (UPS) system (Kratos AXIS ULTRA^{DLD}). A He I (21.2 eV) excitation line was used and a reverse bias of −7.55 V was applied on the samples during the UPS measurement. Moreover, the Au Fermi edge was taken as a reference. The work function Φ was determined by the following relationship:

$$\Phi = hv - \Delta E, \tag{1}$$

where ΔE is the energy difference between Fermi level and secondary electron cutoff, and hv is the ultra-violet (UV) source energy (21.1 eV).[20] The carrier concentration of the SnO film and Si substrate was measured at room temperature using a Hall-effect measurement system (HP-5500C, American Nanometrics). I-V and C-V characteristics of the heterojunctions were measured at room temperature in the dark using a semiconductor parameter analyzer (Keithley 4200-SCS).

Figure 1 shows a representative I-V curve of the p-SnO/n-Si heterojunctions, and the inset shows their schematic structure. The forward turn-on voltage was about ∼1.1 V, and a low leakage current was observed under reverse bias. The forward-to-reverse current ratio was 58 ± 5 at ±2.0 V averaged from more than 10 samples, which is more competitive than the previously reported results based on p-SnO.[13–15]

To in depth understand the electrical behaviors of the p-SnO/n-Si heterojunctions, the ideality factor and the series resistance were deduced from the I-V characteristics, as shown in Figure 2. The ideality factor n could be determined by using the usual junction rectification model in the low bias region

$$I = I_0\left[\exp\frac{qV}{nkT} - 1\right], \tag{2}$$

where I_0 is the maximum reverse current, q is the electronic charge, V is the applied voltage, k is the Boltzmann constant, and T is the absolute temperature. According to the Sah-Noyce-Shockley (SNS) theory, the ideality factor varies between 1.0 and 2.0. However, the ideality factor extracted from experiment is usually larger than 2.0, which was suggested to be due to the presence of interdiffusion, highly strained interface, high series resistance, or parasitic rectifying junctions within the device.[21–26] The ideality factor in this study was about 5.5. The relatively large value might be due to the interdiffusion at the SnO/Si interface, because there is little strain between polycrystalline SnO thin films and Si substrate, as well as a small series resistance of our pn junction. In general, the series resistance R_s has the following relationship with the forward current:[27]

$$I = I_0\exp\left[\frac{q(V - IR_s)}{nkT}\right]. \tag{3}$$

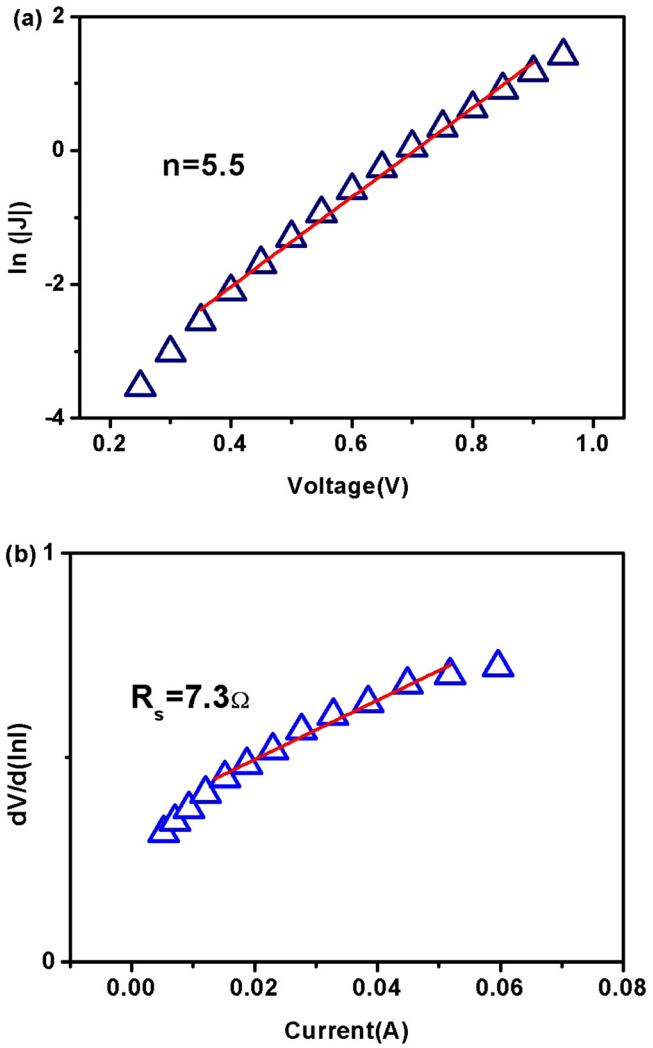

FIG. 2. The linear fit to the ln(|J|) curve (a) and the curve of dV/dln(I)-I (b) for the p-SnO/n-Si heterojunction.

Based on formula (3), the above relation can be further developed as follows:[28]

$$\frac{dV}{dln(I)} = \frac{nkT}{q} + IR_s. \tag{4}$$

So, the R_s can be deduced from the intercept of dV/dln(I) vs. I plot. The extraction of the series resistance in such two-terminal device has already been used. For example, series resistance of 483–533 Ω and 25–45 Ω was derived in the n-ZnO/p-Si and n-ZnSe/p-Si heterojunction, respectively.[29,30] In our case, a series resistance as low as ∼7.3 Ω was obtained.

Figure 3 displays the plot of $1/C^2$-V curve derived from the C-V measurement with a working frequency of 1 MHz. It is linear in the reverse region ranging from 0 to −3 V, confirming that the junction is electrically abrupt. According to Anderson's abrupt junction diffusion model, the relation between the unit area capacitance and applied voltage can be expressed as

$$\frac{1}{C^2} = \frac{2(\varepsilon_P\varepsilon_0 N_P + \varepsilon_N\varepsilon_0 N_N)(V_D - V_a)}{\varepsilon_P\varepsilon_0^2\varepsilon_N q N_P N_N}. \tag{5}$$

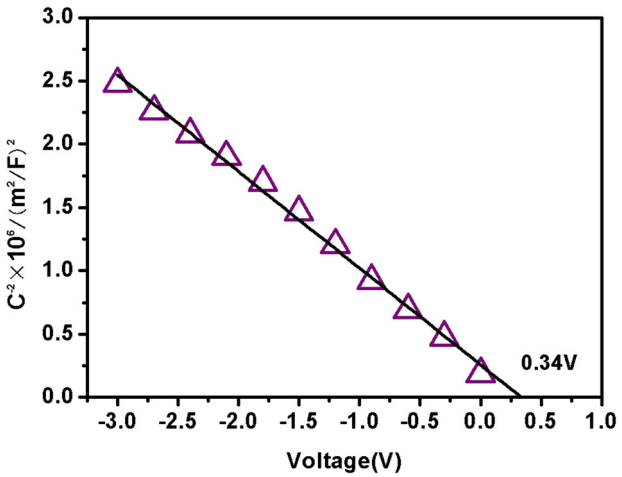

FIG. 3. The linear fit to the $1/C^2$-V curve of the p-SnO/n-Si heterojunction.

Here, C is the unit area capacitance of the heterojunction, V_a is the applied voltage imposed on the electrodes, ε_0 is the vacuum permittivity, and ε_P and ε_N are the relative permittivities of SnO and Si, respectively. The hole concentration N_P in the SnO layer and the electron concentration N_N in the Si wafer were, respectively, determined to be $\sim 1.0 \times 10^{17}$ and $\sim 1.0 \times 10^{19}/cm^3$ according to the Hall-effect measurements. Build-in voltage V_D of 0.34 V can be obtained from x-axis intercept from a linear fit, as shown in Fig. 3. The slope of $1/C^2$-V curve can be expressed as

$$\frac{d(C)^{-2}}{dV_a} = \frac{-2(\varepsilon_P\varepsilon_0 N_P + \varepsilon_N\varepsilon_0 N_N)}{\varepsilon_P\varepsilon_0^2\varepsilon_N q N_P N_N}. \quad (6)$$

Hence, in conjunction with the known parameters, the relative permittivity of SnO can be deduced to be 18.8 ± 1.7 based on the statistic results. The relative permittivity of SnO was reported to be 15 by Ogo *et al.*,[12] but they did not show any detailed information.

It is well known that the band diagram plays an important role in describing the working mechanism of the electric or optoelectronic devices. Essentially, a vital physical picture of a pn junction is the band alignment, which provides basic instruction to the device designers.[31] Figure 4 illustrates the equilibrium energy-band diagram of the p-SnO/n-Si heterojunction, in which the interfacial states as well as the possibly existing ultrathin silicon oxide films between SnO and Si are not taken into considerations. The electron affinity of SnO is 3.7 eV calculated by the relationship $\chi(SnO) = I_P(SnO) - E_g(SnO)$, where the ionization potential of SnO $I_P(SnO)$ and the indirect band gap of SnO $E_g(SnO)$ are, respectively, taken as 4.4 and 0.7 eV.[8,18] The work function of SnO is determined to be 4.3 eV from the UPS measurement, as shown in Figure 5. The parameters related to Si are from the literatures, i.e., the work function of 4.07 eV,[32] the electron affinity of 4.05 eV,[32] and the band gap of 1.12 eV.[18,32] As the electron concentration of Si is much lower than the hole concentration of SnO, the depletion space charge mainly locates at SnO side. It can be derived that the absolute conduction band offset $\Delta E_C = E_C(Si) - E_C(SnO)$ is equal to 0.35 eV, while the valance band offset $\Delta E_V = E_V(Si) - E_V(SnO) = E_g(Si) - E_g(SnO) + \Delta E_C = 0.77$ eV. According to the energy band diagram depicted in Figure 4, an applied voltage $(V_D + |\Delta E_C/q|)$ of 0.69 V is necessary for transporting electrons from Si to SnO, while $(V_D + |\Delta E_V/q|)$ of 1.12 V for transporting holes from SnO to Si. Based on the established energy band diagram, the forward I-V properties of the p-SnO/n-Si heterojunction can be divided into three zones. As the forward bias is less than 0.69 V, the current is relatively weak because both electrons and holes are blocked. Once the forward bias exceeds 0.69 V, the forward current begins to increase gradually due to the injection of electrons from Si to SnO. When the forward voltage is close to 1.12 V, the heterojunction is totally turned on, because both electrons and holes can contribute to the overall current. The above predicted features such as the three operating zones and the turn-on voltage are in good agreement with the experimental I-V results, implying that the established energy band diagram is convincing.

In summary, p-SnO/n-Si heterojunctions were fabricated, which exhibits a forward turn-on voltage of ~1.1 V and a forward-to-reverse current ratio of 58 ± 5 at ± 2.0 V. The diode parameters, such as series resistance, ideality factor, and build-in voltage, were also determined. The relative permittivity and work function of the SnO films were deduced to be 18.8 ± 1.7 and 4.3 eV, respectively. The

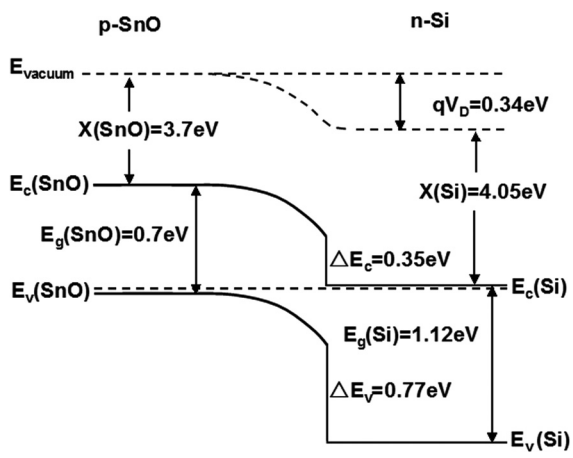

FIG. 4. The energy band diagram of the p-SnO/n-Si heterojunction.

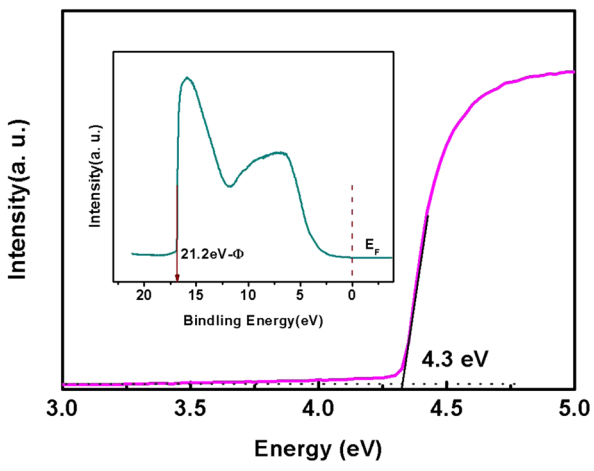

FIG. 5. He I UPS spectra of the SnO films deposited by e-beam evaporation.

established energy band diagram of the heterojunction could account for their I-V characteristics very well. These results would deepen our knowledge of the fundamental physical properties of the SnO material.

This work was supported by the National Natural Science Foundation of China (Grant Nos. 61274095 and 61474126) and the Chinese National Program on Key Basic Research Project (2012CB933003).

[1]K. Wetchakun, T. Samerjai, N. Tamaekong, C. Liewhiran, C. Siriwong, V. Kruefu, A. Wisitsoraat, A. Tuantranont, and S. Phanichphant, Sens. Actuators, B **160**, 580 (2011).
[2]K. Arshak, O. Korostynska, and D. Morris, Mater. Sci. Eng., B **118**, 275 (2005).
[3]R. Jose, V. Thavasi, and S. Ramakrishna, J. Am. Ceram. Soc. **92**, 289 (2009).
[4]M. Reddy, G. Subba Rao, and B. Chowdari, Chem. Rev. **113**, 5364 (2013).
[5]M. R. Hoffmann, S. T. Martin, W. Y. Choi, and D. W. Bahnmann, Chem. Rev. **95**, 69 (1995).
[6]T. Kamiya and H. Hosono, NPG Asia Mater. **2**, 15 (2010).
[7]M. Z. Iqbal, F. P. Wang, M. Y. Rafique, S. Ali, R. U. Din, M. H. Farooq, M. Khan, and M. Ali, J. Nanosci. Nanotechnol. **13**, 1773 (2013).
[8]Y. Ogo, H. Hiramatsu, K. Nomura, H. Yanagi, T. Kamiya, M. Hirano, and H. Hosono, App. Phys. Lett. **93**, 032113 (2008).
[9]L. Y. Liang, Z. M. Liu, H. T. Cao, W. Y. Xu, X. L. Sun, H. Luo, and K. Cang, J. Phys. D: Appl. Phys. **45**(8), 085101 (2012).
[10]L. Y. Liang, Z. M. Liu, H. T. Cao, Z. Yu, Y. Y. Shi, A. H. Chen, H. Z. Zhang, Y. Q. Fang, and X. L. Sun, J. Electrochem. Soc. **157**(6), H598 (2010).
[11]J. A. Caraveo-Frescas, P. K. Nayak, H. A. Al-Jawhari, D. B. Granato, U. Schwingenschlögl, and H. N. Alshareef, ACS Nano **7**, 5160 (2013).
[12]Y. Ogo, H. Hiramatsu, K. Nomura, H. Yanagi, T. Kamiya, M. Kimura, M. Hirano, and H. Hosono, Phys. Status Solidi A **206**, 2187 (2009).
[13]H. Hosono, Y. Ogo, H. Yanagi, and T. Kamiya, Electrochem. Solid-State Lett. **14**, H13 (2011).
[14]F. S. Tsai, S. J. Wand, Y. C. Tu, Y. W. Hsu, C. Y. Kuo, Z. S. Lin, and R. M. Ko, Appl. Phys. Express **4**, 025002 (2011).
[15]K. Sanal and M. Jayaraj, Mater. Sci. Eng., B **178**, 816 (2013).
[16]A. K. Sinha, P. K. Manna, M. Pradhan, C. Mondal, S. M. Yusuf, and T. Pal, RSC Adv. **4**, 208 (2014).
[17]E. Fortunato, R. Barros, P. Barquinha, V. Figueiredo, S. H. K. Park, E. Elamurugu, C. S. Hwang, and R. Martins, Appl. Phys. Lett. **97**, 052105 (2010).
[18]N. F. Quackenbush, J. P. Allen, D. O. Scanlon, S. Sallis, J. A. Hewlett, A. S. Nandur, B. Chen, K. E. Smith, C. Weiland, D. A. Fischer *et al.*, Chem. Mater. **25**, 3114 (2013).
[19]L. Y. Liang, Z. M. Liu, H. T. Cao, and X. Q. Pan, ACS Appl. Mater. Interfaces **2**, 1060 (2010).
[20]Y. Park, V. Choong, Y. Gao, B. R. Hsieh, and C. W. Tang, Appl. Phys. Lett. **68**, 2699 (1996).
[21]J. H. Hao, J. Gao, Z. Wang, and D. P. Yu, Appl. Phys. Lett. **87**, 131908 (2005).
[22]X. H. Wei, W. Huang, Z. B. Yang, and J. H. Hao, Scr. Mater. **65**, 323 (2011).
[23]M. Cavas, R. K. Gupta, A. A. Al-Ghamdi, Z. Serbetci, Z. H. Gafer, F. El-Tantawy, and F. Yakuphanoglu, J. Electroceram. **31**, 260 (2013).
[24]Z. B. Yang, W. Huang, and J. H. Hao, Appl. Phys. Lett. **103**, 031919 (2013).
[25]S. Friedrich-Leonhard, W. Holger von, and G. Marius, Appl. Phys. Lett. **102**, 092109 (2013).
[26]C.-X. Wang, G.-W. Yang, H.-W. Liu, Y.-H. Han, J.-F. Luo, C.-X. Gao, and G.-T. Zou, Appl. Phys. Lett. **84**, 2427 (2004).
[27]S. K. Cheung and N. W. Cheung, Appl. Phys. Lett. **49**, 85 (1986).
[28]R. K. Gupta, K. Ghosh, and P. K. Kahol, Physica E **41**, 617 (2009).
[29]S. Sharma and C. Periasamy, Superlattices Microstruct. **73**, 12 (2014).
[30]S. Darwish, A. S. Riad, and H. S. Soliman, Semicond. Sci. Technol. **11**, 96 (1996).
[31]H. Kroemer, Phys. Scr. T **68**, 10 (1996).
[32]E. K. Liu, B. S. Zhu, and J. S. Luo, *The Physics of Semiconductors* (Publishing House of Electronics Industry, 2012).
[33]See supplementary material at http://dx.doi.org/10.1063/1.4916664 for the optimization of the rapid annealing temperature.